

DIVERTOR DETACHMENT IN THE PRE-FUSION POWER OPERATION PHASE IN ITER DURING APPLICATION OF RESONANT MAGNETIC PERTURBATIONS FOR ELM SUPPRESSION

H. Frerichs

Department of Engineering Physics, University of Wisconsin – Madison
Madison, WI 53706, USA

Email: hfrerichs@wisc.edu

Y. Feng

Max-Planck-Institut für Plasmaphysik, Association EURATOM-IPP
17491 Greifswald, Germany

L. Li

College of Science, Donghua University
Shanghai 201620, China

Y. Q. Liu

General Atomics
PO Box 85608, San Diego, CA 92186-5608, USA

A. Loarte

ITER Organization
Route de Vinon-sur-Verdon, CS 90 046, 13067 St Paul Lez Durance Cedex, France

R. A. Pitts

ITER Organization
Route de Vinon-sur-Verdon, CS 90 046, 13067 St Paul Lez Durance Cedex, France

D. Reiter

Institute for Laser and Plasma Physics, Heinrich-Heine-University
40225 Düsseldorf, Germany

O. Schmitz

Department of Engineering Physics, University of Wisconsin – Madison
Madison, WI 53706, USA

Abstract

Recent advancements of three dimensional plasma boundary modelling (EMC3-EIRENE) offer a first analysis of resonant magnetic perturbation (RMP) effects on divertor detachment in the Pre-Fusion Power Operation (PFPO) phase in ITER. Simulations are based on MARS-F calculations for plasma response to external RMPs, and show that the footprint on the divertor targets may be of similar size or larger as for the vacuum RMP approximation despite screening of resonances. The size of the magnetic footprint varies with plasma rotation in the MARS-F calculation, and may exceed the dedicated high heat flux region on the vertical outer target. While Ne seeding is found to mitigate non-axisymmetric heat loads, it becomes significantly less effective if the magnetic footprint extends far onto the rounded baffle on the outer target.

1 INTRODUCTION

The prospect of magnetic fusion energy is the drive for the ITER project as a stepping stone towards a future reactor. At the forefront of science and engineering, a number of challenges need to be overcome. Among the grand challenges for successful operation of ITER are the control of steady state heat loads and suppression of transient heat loads from edge localized instabilities (ELMs). It is anticipated that 100 MW of power need to be exhausted from the core plasma through the very thin scrape-off layer just outside the magnetic separatrix. Without a mitigation strategy, plasma facing components will experience heat loads that exceed their capabilities by far. Therefore, extensive simulations have been performed to design the ITER divertor [1] for operation in a partially detached state (i.e. reduced particle and heat loads on divertor targets) [2,3]. The

backbone of this design process is the SOLPS package (SOLPS-4.3 and later SOLPS-ITER) [4] for modelling of the plasma boundary. SOLPS exploits the traditional approximation of axisymmetry in tokamak configurations which allows to simplify the model equations to two dimensions for efficiency.

The ITER divertor relies heavily on these predictions, but they do not take into account suppression of ELMs by application of external resonant magnetic perturbations (RMPs) – today’s most promising strategy. ITER will be equipped with 3 rows of 9 external window frame coils which can be operated with different toroidal symmetries and spectral components. Successful ELM suppression by RMPs has been demonstrated in many present devices [5,6,7], but that implies breaking of the continuous toroidal symmetry of the configuration. Three dimensional plasma boundary models have been developed for stellarator configurations and adapted to RMP tokamak configurations over the years [8], but numerical access to detached divertor plasmas has only been achieved recently [9].

Despite promising solutions for each of the two challenges described above, it remains unclear if they remain compatible with each other as present machines cannot access relevant conditions for both at the same time. With recent advancements of the EMC3-EIRENE package we can offer a first analysis of the impact of RMPs on divertor detachment in the Pre-Fusion Power Operation (PFPO) phase in ITER. In this phase, ITER will operate at lower power (30 MW), reduced field (1.8 T) and plasma current (5 MA), but at the same $q_{95} = 3.1$ as anticipated for the Fusion Power Operation (FPO) phase with a burning plasma ($Q = 10$). This is an ideal test bed for RMP application, because resonances will be at similar radial positions throughout the plasma (resulting in similar magnetic field structures in the plasma boundary – at least in vacuum RMP approximation). At the same time, power handling requirements are not as restrictive as for the FPO phase, and so it is possible to explore the transition from attached to detached states with and without impurity seeding for supplemented dissipation.

Our focus is on application of RMPs with toroidal symmetry $n = 3$ at a relative phasing between rows that has been optimized for a large X-point displacement as proxy for ELM control. We will begin with a brief description of the EMC3-EIRENE model for the plasma boundary in section 2 and then go into plasma response effects in section 3. The impact of RMPs on supplemented dissipation from Ne seeding is investigated in section 4.

2 PLASMA BOUNDARY MODELLING

Evaluation of the impact of magnetic perturbations on the boundary plasma and resulting divertor loads requires a three dimensional model such as EMC3-EIRENE. Traditionally, plasma boundary modelling is based on a given magnetic geometry (set by the axisymmetric equilibrium field \mathbf{B}_{equi}) on which balance equations for particles, momentum and energy are solved. Quasi-neutrality and anomalous cross-field transport for particles and energy are common assumptions, and model equations are constrained by total particle throughput (gas puff and core fuelling vs. pumping) and total power exhaust from the core through the scrape-off layer.

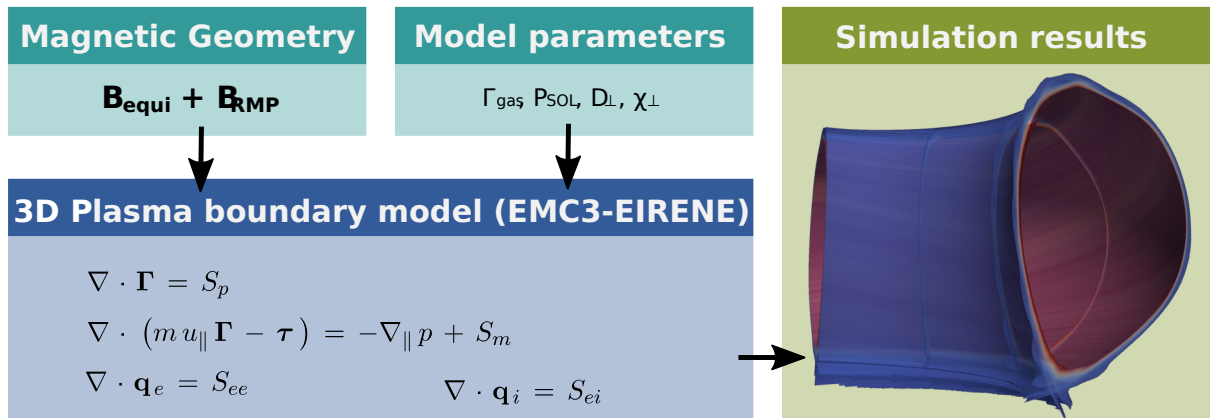


Fig 1: The EMC3-EIRENE model for a 3D plasma boundary: the magnetic geometry is required input along with model parameters for particle throughput, power entering the SOL and anomalous cross-field transport.

EMC3-EIRENE (Fig. 1) extends the traditional approach into three dimensions: here the magnetic geometry is defined by perturbed field lines (reconstructed from a field aligned grid). For a long time, the magnetic

geometry was approximated based on the externally applied perturbation alone (vacuum RMP approximation), but plasma response effects can be taken into account as long as they are provided by other models. EMC3-EIRENE itself is agnostic of the source of the perturbation field \mathbf{B}_{RMP} as it reconstructs field lines from a specifically designed grid [10, 11]. Such a grid is constructed before the simulation with the field line tracing suite FLARE where the total perturbation field including plasma response can be plugged in instead of the externally applied field. All plasma response fields in this paper are from a recent database of cases [12] based on MARS-F [13], a single fluid, linearized, resistive magneto-hydrodynamic model. At this point, no feedback from the plasma boundary simulation on the plasma response calculation is taken into account. As a preliminary step, however, the impact of model assumptions in the plasma response calculation will be addressed in section 3.2.

3 PLASMA RESPONSE EFFECTS

The ideal plasma is expected to shield external perturbations, but finite resistivity allows for reconnection of field lines and formation of island chains where the helical pitch $q = m/n$ (safety factor) is a rational value. Externally applied perturbations can thus lead to formation of a set of fairly large island chains, and those may overlap at the edge where resonances are located relatively close to each other. Overlapping island chains result in a layer with chaotic (also referred as stochastic) field line trajectories. The perturbed magnetic separatrix begins to oscillate in a helical pattern and guides field lines from the chaotic region towards the divertor targets. This acts as a new exhaust channel that can largely replace the traditional scrape-off layer.

3.1 Comparison to Vacuum RMP approximation

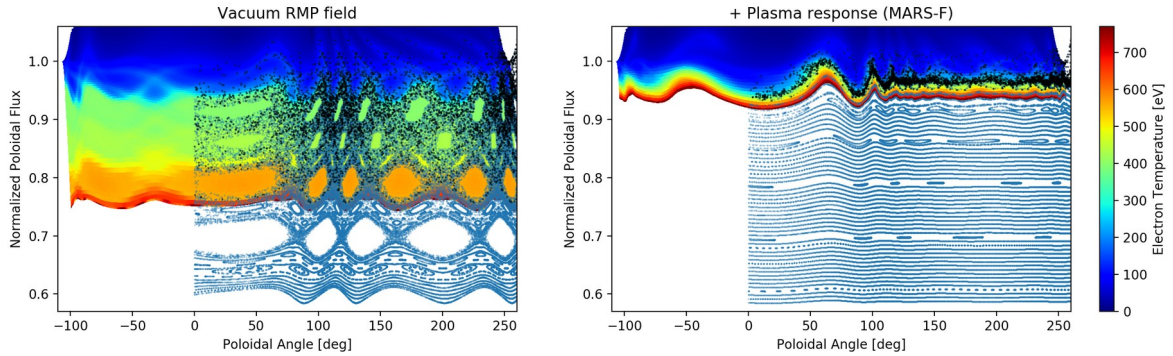


Fig 2: Simulation results for the electron temperature based on the vacuum RMP approximation (left) and with plasma response included (right). Poincaré plots (blue) show the magnetic geometry. The RMP strength is 30 kAt.

Fig. 2 (left) shows simulation results for the electron temperature based on the vacuum RMP approximation. It also includes a Poincaré plot that visualizes the magnetic geometry resulting from external perturbations. The last closed magnetic flux surface is located at $\Psi_N \approx 0.77$ which is taken as inner boundary for the EMC3-EIRENE simulation. Remnant island chains remain throughout the edge, but field lines from the large chaotic layer eventually connect to the divertor targets. The presence of a ‘ghost’ surface (only few field lines pass through) at $\Psi_N \approx 0.82$ can be seen in the resulting temperature which remains largely flat on either side of this surface in the 550 eV and 400 eV range.

Significant screening of resonant fields is recovered in resistive plasma response calculations. The Poincaré plot in Fig. 2 (right) shows that intact flux surfaces exist up to $\Psi_N \approx 0.94$ where the last closed flux surface can support temperatures of about 750 eV. This is about a factor of 2 higher than in the vacuum RMP approximation at the same radial position. Clearly, this reveals the deficit of the vacuum RMP approximation in plasma boundary simulations which is in line with earlier simulations for ITER [14] and DIII-D [15]. However, unlike the explicit screening applied in those earlier simulations, the present screening results are obtained from plasma response calculations in full toroidal geometry. The important difference is that the MARS-F plasma response can include a field amplification near the separatrix as we will discuss later in section 3.2 and Fig. 5. And this field amplification has a significant impact on the field line connection to the divertor targets.

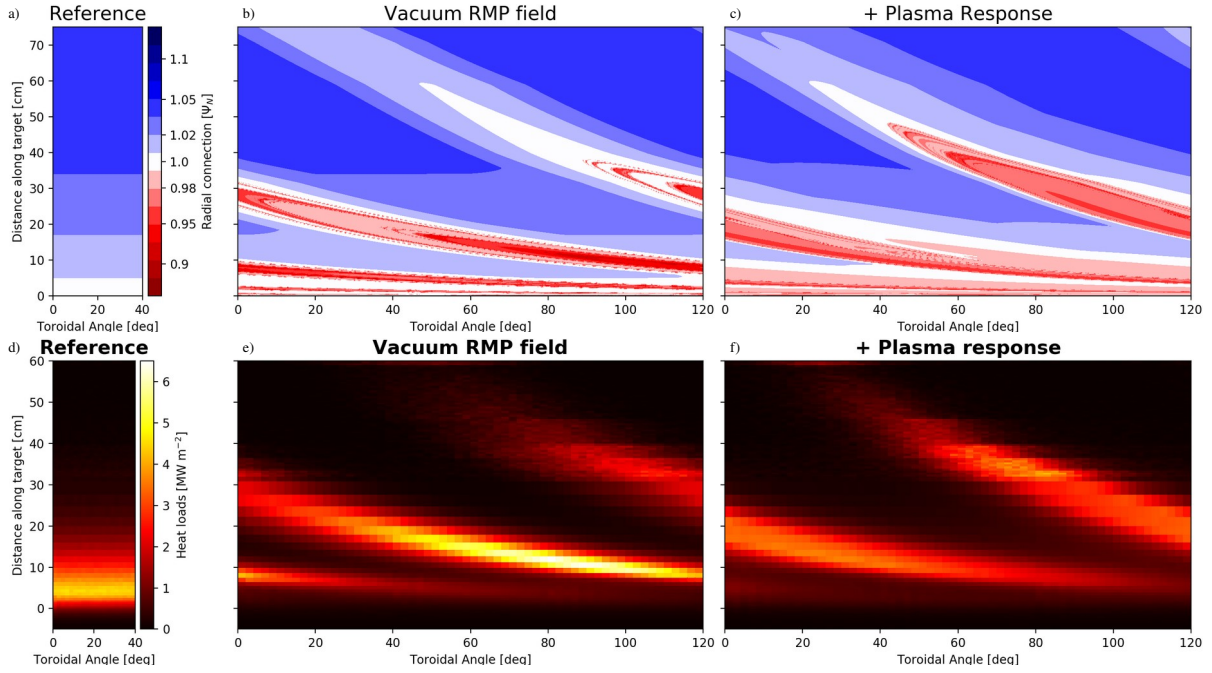


Fig 3: Upper row: magnetic footprint on the outer divertor target, lower row: resulting heat loads at a total particle throughput of $\Gamma_{gas} = 3 \cdot 10^{22} s^{-1}$. RMP application with external field only (vacuum) and with plasma response included is compared to the unperturbed (reference) configuration.

The magnetic footprint on the outer divertor target is shown in the upper row Fig. 3 in terms of the radial connection of field lines. The radial connection R of a field line is defined as the minimum of normalized poloidal flux Ψ_N that a field line encounters along its way. An unperturbed field line never leaves its associated flux surface, and so contour lines of R are equivalent to the flux surface contours in the unperturbed configuration. White colours indicate the thin layer outside the separatrix (near SOL) with significant heat flux upstream. On the divertor target, heat flux is spread further out (into the light blue regions), as can be seen by comparing Fig. 3 a) and d) while no significant heat flux reaches the far SOL (darker blue colours).

As introduced above, the perturbed magnetic separatrix guides field lines from the bulk plasma ($\Psi_N < 1$) towards the divertor targets. This is evident in Fig. 3 b) and c) from the red colours. As the vacuum RMP field leads to a large chaotic domain, field lines may connect to the target from deep within the bulk plasma (dark red colours). As can be seen from the corresponding EMC3-EIRENE simulation for the same gas fuelling rate, the deep connections results in localized heat loads which are both higher than in the unperturbed reference case and localized further outwards at a distance of ~ 10 cm from the separatrix strike point of the unperturbed case. Almost all heat flux is exhausted along perturbed field lines from the bulk plasma (red), while the traditional scrape-off layer (white, blue) is more of an appendix with ‘overflow’ from cross-field transport through the perturbed separatrix.

Despite screening of most resonances throughout the plasma, the localized field amplification of the plasma response results in a magnetic footprint which moderately exceeds that of the vacuum RMP approximation, as can be seen by comparing Fig. 3 b) and c). Nevertheless, as a result of the screening response, the radial connection is not as deep (lighter red colours). Consequently, heat loads are not as peaked and more evenly distributed, although the maximum occurs even further way at a distance of ~ 32 cm from the separatrix strike point of the unperturbed configuration. While there are obvious differences in the resulting heat load pattern with RMPs, the outline is still fairly comparable. Therefore, experimental observations restricted to the heat load pattern may not provide the correction conclusion about the vacuum-likeness of the magnetic geometry. Including upstream information along the comparison of Fig. 2 will provide a more robust answer to that.

A common observation for the RMP configurations is that the original near SOL domain exhibits virtually no heat loads which suggests an earlier onset of detachment here. Power balance along field lines between the divertor entrance and targets indicates that most of the heat flux is dissipated by both cross-field diffusion and

excitation (and subsequent photon emission) of neutral gas [16]. The earlier onset of detachment is consistent with a lower heat flux upstream resulting from distributing P_{SOL} over perturbed field lines.

3.2 Impact of plasma response model parameters

As screening of resonant fields competes with field amplification at the plasma edge, the resulting magnetic footprint can be sensitive to the parameters that determine this balance. The plasma response case discussed above is based on the assumption of low rotation, which is consistent with expectations for ITER. Nevertheless, 3 cases have been analysed with different assumptions for the ratio of momentum to energy confinement times τ_ϕ/τ_E which result in different rotation profiles (computed by ASTRA as input for the MARS-F calculations). Fig. 4 shows these rotation profiles which will be referred to as low (red), moderate (green) and high (blue) rotation in the following.

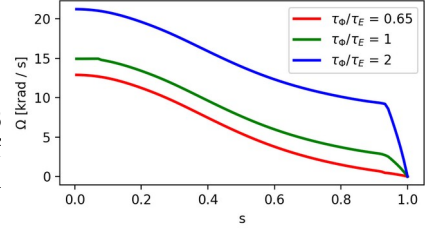


Fig 4: Rotation profiles used in MARS-F plasma response modelling.

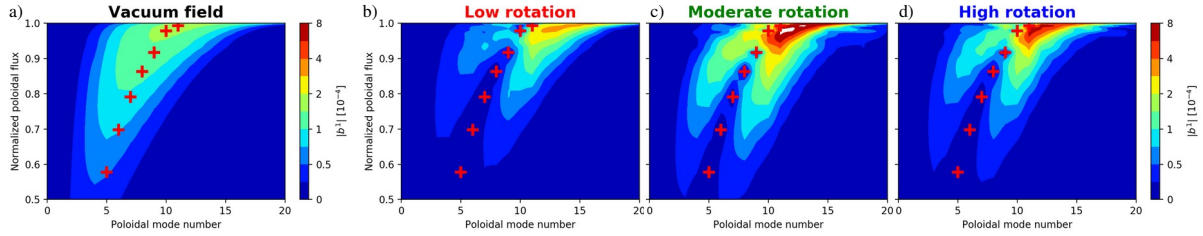


Fig 5: Spectrum of external perturbation field (a) and total perturbation field including plasma response resulting from different rotation profiles (b-d).

For characterization of the perturbation field \mathbf{B}_{RMP} (or more precisely its radial component) we now turn to the poloidal Fourier spectrum of the perturbed flux $\Phi = \mathbf{J} \cdot \mathbf{B}_{\text{RMP}}$ where \mathbf{J} is the surface Jacobian. The normalized harmonics of the perturbation are evaluated in straight field line coordinates (θ, φ) , and are given by

$$b_{mn}^1 = \frac{1}{R_0^2 B_0} \Phi_{mn} \quad \text{where} \quad \Phi_{mn} = \frac{1}{(2\pi)^2} \oint d\vartheta d\varphi \frac{\mathbf{B}_{\text{RMP}} \cdot \nabla \psi}{B \cdot \nabla \vartheta} e^{-i(m\vartheta - n\varphi)}.$$

Here, B_0 is the toroidal field at the magnetic axis and R_0 is the corresponding major radius. The radial dependence of b_{mn}^1 is shown in Fig. 5 a) for the external perturbation field with toroidal symmetry $n = 3$. The resonant nature of the external perturbation field is apparent from the red symbols which mark the position of the resonances determined by the helical pitch $q = m/n$ of the equilibrium field. The relatively large resonant fields of the externally applied perturbation are responsible for the island chains and wide stochastic region in Fig. 2 a).

The spectrum of the total perturbation field with plasma response included is shown in Fig. 5 b) – d) for the 3 different rotation cases. Screening of the resonant field is found for all cases throughout most of the plasma, and this is the response that results in the much narrower perturbed boundary in Fig. 2 b) and shallower radial connection in Fig. 3 c). Nevertheless, amplification of the (mostly non-resonant) fields near the edge is found as well. The difference between the cases, however, is the level of field amplification: moderate amplification is found for the low rotation case, while strong amplification is found for the moderate and high rotation cases. Even though the moderate (green) rotation profile is closer to the low (red) rotation profile in Fig. 4, the resulting field amplification in Fig. 5 is closer to that of the high (blue) rotation case. This sensitivity at low to moderate rotation requires further investigation.

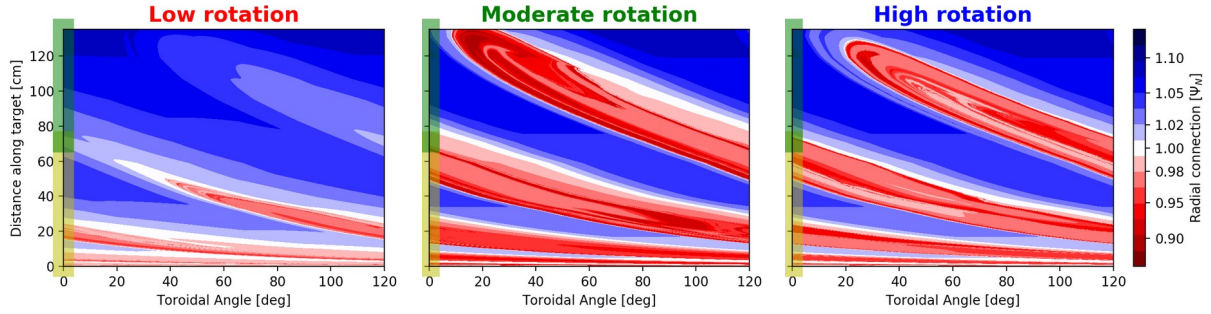


Fig 6: Magnetic footprints resulting from plasma response (MARS-F) calculations for the low, moderate and high rotation cases. The low rotation case is the same as Fig. 3 c). The yellow bar marks the dedicated high heat flux region on the divertor target where leading edges of the tungsten mono-blocks are shielded, while the green bar marks the rounded divertor baffle with lower tolerances for heat loads.

The strong amplification in the moderate and high rotation cases is directly reflected in the resulting size of the magnetic footprint, as can be seen in Fig. 6. Both of these cases exhibit magnetic footprints where field lines connect from the bulk plasma to the rounded divertor baffle up to 120 cm away from the original separatrix strike point. While the vertical target (highlighted in yellow in Fig. 6) has a rather high tolerance for heat loads from precise alignment and shaping of the tungsten mono-blocks (MBs) for protection of leading edges, the rounded baffle region (highlighted in green) has a much lower tolerance despite being constructed from the same material.

The resulting heat loads for the high rotation plasma response case¹ are shown in Fig. 7: virtually no heat loads appear in the original strike region < 20 cm, but significant heat loads $\sim 3 \text{ MW m}^{-2}$ appear at the outermost part of the magnetic footprint far beyond the dedicated high heat flux region (yellow). Note that at a field line incident angle of 2.7 deg on the (unshaped) target surface, already a small heat load of $\sim 0.5 \text{ MW m}^{-2}$ corresponds to a parallel heat flux that would bring 10 MW m^{-2} to exposed edges of the MBs. Therefore, heat loads beyond the vertical target should be avoided, or at least adequately mitigated. As heat loads on the rounded baffle are toroidally localized to a region of about 20 deg, it appears that sufficient mitigation is just possible with slow (several Hz) rotation of the perturbation field. However, it should be noted that such rotation would significantly reduce the lifetime of the coil system, and so this option should only be considered as a last resort. Impurity seeding for supplemented power dissipation may be an alternative, especially since this is already anticipated for the (unperturbed) symmetric configuration during the FPO phase where 100 MW need be exhausted through the SOL instead of 30 MW.

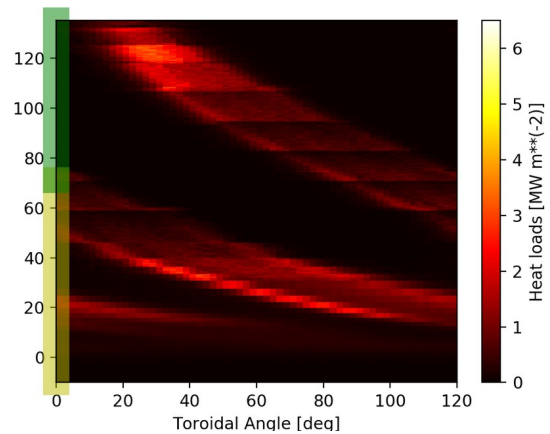


Fig 7: Heat loads for the high rotation plasma response case from Fig. 6 c). Note the same colour bar as for heat loads in Fig. 3 d) – f) is used.

4 IMPURITY SEEDING FOR SUPPLEMENTAL POWER DISSIPATION

EMC3-EIRENE may include the impact of trace impurities on the boundary plasma, where “trace” means that the only impact on the main plasma species comes from an additional cooling term $S_{ee,imp}$ in the energy balance for electrons in Fig. 1. These power losses are caused by collisional excitation (and ionization), and subsequent photon emission. In the following simulations, Ne impurities are seeded through a gas puff from the top of the device along with the main species, while pumping of impurities is treated in an implicit approximation through a reflection coefficient of 99% at the divertor targets. The source strength is scaled to match an average concentration of 1% at $\Psi_N = 1$.

¹ Even though the high rotation case may be less likely than the low or moderate rotation case, the similar footprint size of the moderate rotation case suggests that such a magnetic configuration should not be discarded.

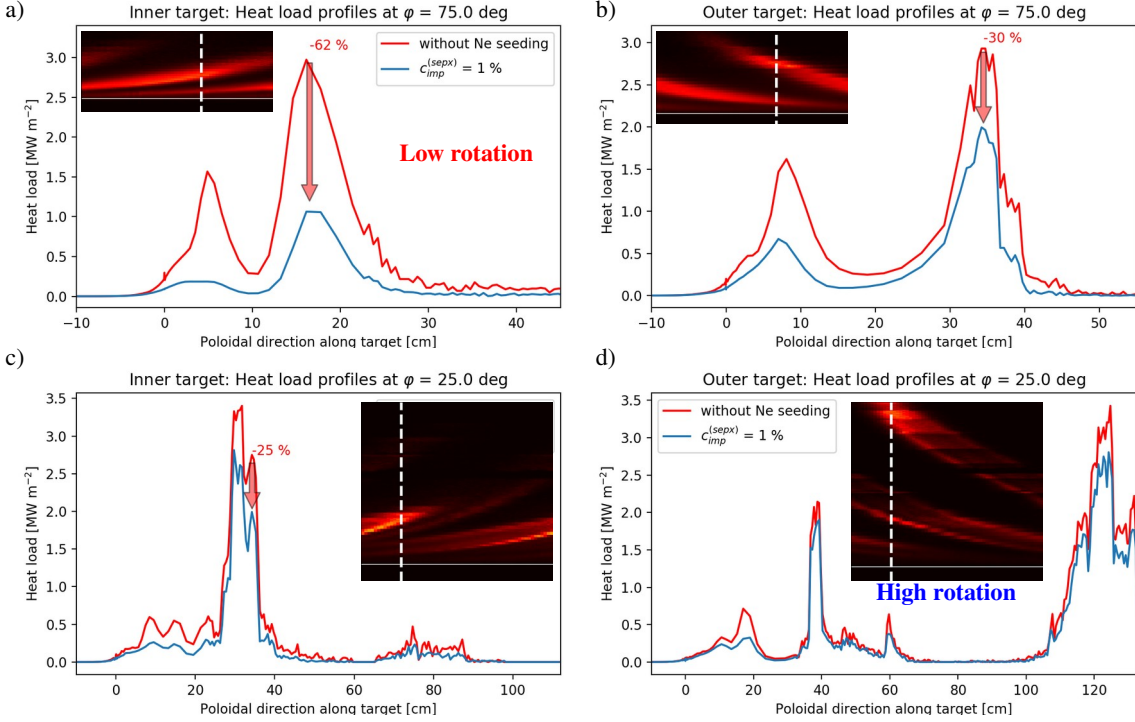


Fig 8: Heat load profiles at the inner (left) and outer (right) divertor targets with (blue) and without (red) Ne seeding for the low rotation (upper row) and high rotation case (lower row).

Resulting heat loads are shown in Fig. 8 for both inner and outer targets for the low rotation case in which the magnetic footprint stays on the vertical outer target (upper row), and for the high rotation case in which the magnetic footprint extends onto the rounded divertor baffle. Our focus here is on the impact on the outermost non-axisymmetric peak, because heat loads to the original strike zone are already significantly reduced. Toroidal locations for the profiles are chosen such that far-SOL peaks are captured as can be seen in the insets for guidance. It can be seen in Fig. 8 b) that a moderate reduction (-30 %) of the outermost peak can be achieved on the outer target with Ne seeding in the low rotation case. This is promising, keeping in mind that the PFPO phase has lower upstream pressure than the FPO phase which may limit divertor density and impurity radiation. This is supported by Fig. 8 a) which shows a stronger reduction of the peak heat load by -60 % at the inner target in the same simulation, consistent with higher density and lower temperature here.

Unfortunately, the beneficial impact of Ne seeding is much less effective for the high rotation plasma case. It can be seen in Fig. 8 d) that a small reduction of the heat load onto the rounded baffle is possible, but not enough to be tolerable for exposed edges on the MBs. The lower dissipation efficiency is related to the lower density and higher temperatures at this location compared to the outermost peak in the low rotation case in Fig. 8 b). Even on the inner target, the temperature at the heat load peak remains high and only a small reduction of heat load from impurity radiation is found.

5 CONCLUSIONS

A good understanding of the plasma response is key for reliable predictions of divertor heat and particles fluxes. Screening of resonant fields throughout most of the plasma competes with field amplification near the separatrix, and this balance determines the radial connection of field lines into the bulk plasma and the size of the magnetic footprint on the divertor targets. The significant difference between low and moderate rotation cases calls for further sensitivity studies. While at low rotation, the outermost peak on the divertor targets can be reduced by 30 % on the outer target and 60 % on the inner target, power dissipation becomes significantly less effective if the magnetic footprint extends beyond the vertical target onto the rounded baffle on the outer target where tolerances for heat loads are much lower. This is likely caused by the lower density and higher temperature at those peaks, which may be an implication of the lower upstream density that results at the same Γ_{gas} in these simulations. Further mitigation of heat loads may be possible at higher Γ_{gas} (and upstream density), higher impurity concentration, and with fine tuning of the coil parameters while maintaining ELM control.

ACKNOWLEDGEMENTS

This work was supported by the U.S. Department of Energy under awards No. DE-SC0020357, DE-SC0020428, DE-SC0020425, and by the College of Engineering at the University of Wisconsin – Madison. This work was conducted under the auspices of the ITER Scientist Fellow Network. The views and opinions expressed herein do not necessarily reflect those of the ITER Organization.

REFERENCES

- 1 PITTS, R. A. et al., “Physics basis for the first ITER tungsten divertor”, NME 20 (2019) 100696
- 2 KRASHENINNIKOV, S. I and KUKUSHKIN, A. S., “Physics of ultimate detachment of a tokamak divertor plasma”, J. Plasma Phys., 83 (2017) 155830501
- 3 STANGEBY, P. C., “Basic physical processes and reduced models for plasma detachment”, Plasma Phys. Control. Fusion, 60 (2018) 044022
- 4 KUKUSHKIN, A. S. et al., “Finalizing the ITER divertor design: The key role of SOLPS modeling”, Fusion Eng. Des., 86 (2011) 2865
- 5 EVANS, T. E. Evans et al., “Suppression of Large Edge-Localized Modes in High-Confinement DIII-D Plasmas with a Stochastic Magnetic Boundary”, Phys. Rev. Lett., 92 (2004) 235003
- 6 LIANG, Y et al., “Active Control of Type-I Edge-Localized Modes with n=1 Perturbation Fields in the JET Tokamak”, Phys. Rev. Lett., 98 (2007) 265004
- 7 SUTTROP, W. et al, “First Observation of Edge Localized Modes Mitigation with Resonant and Nonresonant Magnetic Perturbations in ASDEX Upgrade”, Phys. Rev. Lett., 106 (2011) 225004
- 8 FENG, Y. et al., “Recent Improvements in the EMC3-Eirene Code”, Contrib. Plasma Phys. 54 (2014) 426
- 9 FRERICHS, H. et al., “Stabilization of EMC3-EIRENE for detachment conditions and comparison to SOLPS-ITER”, NME 18 (2019) 62
- 10 FENG, Y. et al., “A simple highly accurate field-line mapping technique for three-dimensional Monte Carlo modeling of plasma edge transport”, Phys. Plasmas 12 (2005) 052505
- 11 FRERICHS, H. et al., “Block-structured grids in Lagrangian 3D edge plasma transport simulations”, Comput. Phys. Commun. 181 (2010) 61
- 12 LI, L. et al., “Modeling 3D plasma boundary corrugation and tailoring toroidal torque profiles with resonant magnetic perturbation fields in ITER”, Nucl. Fusion 59 (2019) 096038
- 13 LIU, Y. Q. et al., “Feedback stabilization of nonaxisymmetric resistive wall modes in tokamaks. I. Electromagnetic model”, Phys. Plasmas, 7 (2000) 3681
- 14 SCHMITZ, O. et al., “Three-dimensional modeling of plasma edge transport and divertor fluxes during application of resonant magnetic perturbations on ITER”, Nucl. Fusion 56 (2016) 066008
- 15 FRERICHS, H. et al., “Impact of screening of resonant magnetic perturbations in three dimensional edge plasma transport simulations for DIII-D”, Phys. Plasmas 19 (2012) 052507
- 16 FRERICHS, H. et al., “Detachment in fusion plasmas with symmetry breaking magnetic perturbation fields”, Phys. Rev. Lett 125 (2020) 155001